

Spin-Hall magnetoresistance and spin Seebeck effect in spin-spiral and paramagnetic phases of multiferroic CoCr_2O_4 films

A. Aqeel,¹ N. Vlietstra,¹ J. A. Heuver,¹ G. E. W. Bauer,^{2,3} B. Noheda,¹ B. J. van Wees,¹ and T. T. M. Palstra^{1,*}

¹*Zernike Institute for Advanced Materials, University of Groningen,
Nijenborgh 4, 9747 AG Groningen, The Netherlands*

²*Institute for Materials Research and WPI-AIMR,
Tohoku University, Sendai, Miyagi 980-8577, Japan*

³*Kavli Institute of NanoScience, Delft University of Technology, Lorentzweg 1, 2628 CJ Delft, The Netherlands*

(Dated: March 2, 2024)

We report on the spin-Hall magnetoresistance (SMR) and spin Seebeck effect (SSE) in multiferroic CoCr_2O_4 (CCO) spinel thin films with Pt contacts. We observe a large enhancement of both signals below the spin-spiral ($T_s = 28$ K) and the spin lock-in transitions ($T_{\text{lock-in}} = 14$ K). The SMR and SSE response in the spin lock-in phase are one order of magnitude larger than those observed at the ferrimagnetic transition temperature ($T_c = 94$ K), which indicates that the interaction between spins at the Pt|CCO interface is more efficient in the non-collinear magnetic state below T_s and $T_{\text{lock-in}}$. At $T > T_c$, magnetic field-induced SMR and SSE signals are observed, which can be explained by a high interface susceptibility. Our results show that the spin transport at the Pt|CCO interface is sensitive to the magnetic phases but cannot be explained solely by the bulk magnetization.

PACS numbers:

Keywords:

I. INTRODUCTION

Ferro (ferri) magnetic insulators (FMI) with normal metallic (NM) contacts that support the spin Hall effect (SHE) and its inverse (ISHE) open new functionalities in the field of spintronics. The SHE refers to a charge current that induces a transverse spin current, which can be injected to actuate a metallic or insulating ferromagnet. The ISHE converts a spin current pumped out of a ferromagnet into a transverse charge current in the normal metal. These concepts have been confirmed by many experiments on FMI|NM bilayers of a magnetic insulator (usually yttrium iron garnet) and a heavy normal metal (usually platinum), for example spin-pumping by ferromagnetic resonance [1–4], the spin Seebeck effect (SSE) [5–8], the spin Peltier effect [9] and the spin Hall magnetoresistance (SMR) [10–15]. In the SMR, both SHE and the ISHE act in a concerted manner to allow electrical detection of the FMI magnetization direction. The SSE refers to the conversion of thermal excitations of the magnetic order parameter (spin waves or magnons) into a spin current pumped into NM and detected by the ISHE. The SSE and the SMR have been investigated up to now only for a limited number of insulating ferrimagnets (garnets and spinels) with collinear magnetizations and recently, in an antiferromagnetic insulator [16]. However, magnetic insulators come in a large variety of magnetic order. Especially fascinating are non-collinear magnets with competing magnetic interactions (spin frustration) induced by competing next-nearest neighbor exchange. Alternatively, the spin-orbit coupling, such as the Moriya-Dzyaloshinskii interaction favor complex spiral configurations and skyrmion order. While the coupling of non-collinear magnetizations with spin, charge and heat transport is currently one of the hottest subjects in magnetism, its role in the SMR and SSE appears to have not been studied yet.

Non-collinear magnetism emerges when the second nearest neighbor magnetic interactions are of the same order as the first one, generating geometrical frustration that favors spin canting. Various spin-spiral orders, like proper screw, cycloidal, longitudinal-conical and transverse-conical spiral, have been observed. The cycloidal and the transverse-conical spiral orders break the inversion symmetry and induce a spontaneous electrical polarization, making these spiral magnetic systems multiferroic [17–21]. Here, we focus on non-collinear and multiferroic CoCr_2O_4 (CCO) thin films, reporting to the best of our knowledge first experimental observation of the SMR and the SSE in the Pt|CCO system for a wide range of temperatures including the ferrimagnetic and the spin-spiral phases.

CCO is one of the rare multiferroic materials with linear magnetoelectric coupling [22, 23]. It has a normal spinel structure with three sublattices. The Co^{2+} ions are located exclusively in the tetrahedral sites (forming one sublattice) while Cr^{3+} ions reside in the octahedral sites (in two sublattices). The Cr^{3+} ions form a pyrochlore lattice

*Electronic address: [e-mail:]t.t.m.palstra@rug.nl

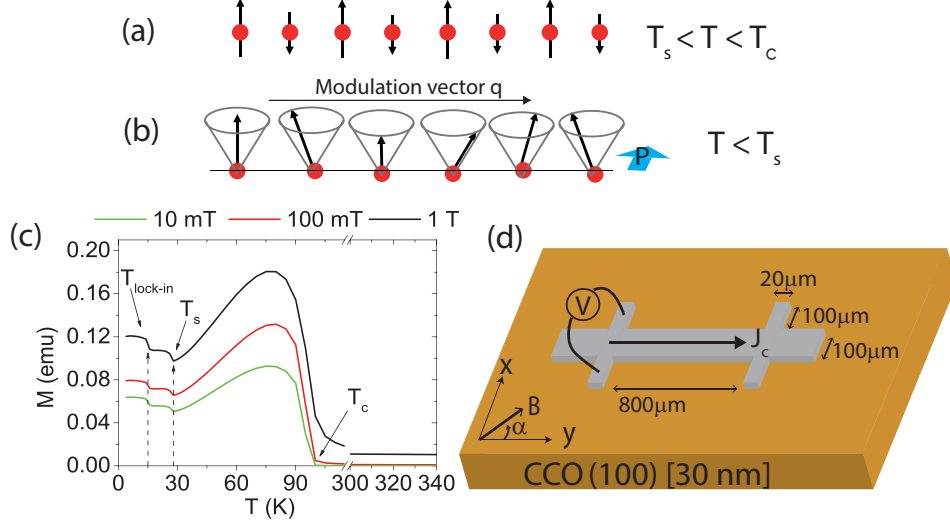


FIG. 1: (a,b) Impression of the types of magnetic order in CCO. (a) Ferrimagnetic state for $T_s < T < T_c$ and (b) transverse conical spiral state for $T < T_s$ with an electrical polarization P . Here, T_c and T_s are the Curie transition temperature to a collinear ferrimagnetic phase and that the spin-spiral transition temperature, respectively. (c) The temperature dependence of the zero-field cooled magnetization of the CCO target powder used for the film deposition for different applied magnetic fields. $T_{\text{lock-in}}$ is the spin lock-in magnetic transition temperature. (d) Device configuration for the transverse resistance (planar Hall effect) measurement of the Pt film on top of CCO.

with magnetic geometrical frustration [24, 25]. Bulk CCO exhibits long-range collinear ferrimagnetic order below $T_c = 93\text{ K} - 95\text{ K}$ [24, 26, 27], with an easy axis of magnetization along the [001]-direction, as illustrated in Fig. 1(a) and (c). At $T_s = 28\text{ K}$, the ferrimagnetic long-range order adopts an additional short-range spiral order as illustrated in Fig. 1(b) and (c), which is known as the spin-spiral phase transition. The conical spiral has 48° , 71° and 28° cone angles with the [001]-direction for the Co-, Cr I- and Cr II- sublattices, respectively. Below T_s , magnetic spin-spirals move the oxygen atoms off-center due to the inverse Dzyaloshinskii-Moriya interaction [26, 28], which results in the appearance of a spontaneous electrical polarization. At $T_{\text{lock-in}} = 14\text{ K}$, the spin-spiral becomes commensurate with the lattice by the spin-lattice coupling, which is known as the spin lock-in transition.

Here, we report a systematic study of the SMR and the SSE in the Pt|CCO bilayers from low to room temperature ($T = 5\text{ K} - 300\text{ K}$). At each temperature, we record the dependence on the angle of an in-plane applied magnetic field. We observe strong effects of the CCO magnetic order with largest signals in the spin lock-in phase at $T < 14\text{ K}$.

II. SAMPLE GROWTH AND CHARACTERISTICS

30-nm-thick CCO films were grown on (001) MgO substrates by pulsed laser deposition (PLD). Sintered ceramic CCO targets [29] were ablated with a KrF excimer laser light with a wavelength of 248 nm and a repetition frequency of 0.5 Hz. During the deposition, the MgO substrates are kept at 500°C in oxygen plasma atmosphere, having a base pressure of 0.01 mbar. Afterwards, the films were cooled down, with 5°C per minute in 0.5 bar O_2 atmosphere. Before further device fabrication, the films were annealed at 200°C for 60 min in an O_2 atmosphere. The crystal structure of the CCO films was determined by x-ray diffraction (XRD), where the rocking curves show high crystalline quality with a Full Width at Half Maximum (FWHM) below 0.03° .

The magnetization of the CCO films was measured by a SQUID magnetometer. The films show an in-plane magnetic anisotropy with a coercive field H_c around 2 T. For temperatures below 50 K, the magnetic transitions are hard to detect due to a large paramagnetic substrate background compared to the small magnetic moment of the thin film (see Appendix A). Nevertheless, SQUID measurements [30, 31] and X-ray resonance magnetic scattering both indicate the same magnetic transitions in thin films as reported for bulk CCO. In order to demonstrate the magnetic transitions in CCO, we measured the temperature dependence of the magnetization of bulk CCO targets used for the film deposition. Fig. 1(c) shows a magnetization of the CCO targets with the same transitions as reported in literature [32]. We carried out transport experiments on Hall-bar structures patterned by electron beam lithography onto which a 4 nm-thick Pt film was deposited by dc-sputtering, as shown in Fig. 1(d).

III. MEASUREMENT TECHNIQUES

SMR and SSE have been measured simultaneously by lock-in detection [33]. Using two Stanford SR-830 Lock-in amplifiers, the first and second harmonic voltage response were recorded separately. To minimize the background voltage, we used the transverse instead of the longitudinal configuration, as schematically shown in Fig. 1(d), which is also referred to as “planar Hall” voltage. The SMR signals scale linearly with the applied current and therefore detected in the Pt resistance of the first harmonic response [33]. The current-induced SSE scales quadratically with the applied current and therefore detected in the second harmonic response. The angular dependence of the SMR and the SSE were studied by rotating an external magnetic field in the plane of the film [34] that above T_c induces a magnetization or (if large enough) aligns the direction of the CCO magnetization below T_c . The in-plane angle α of the magnetic field is defined relative to the current direction along the y -axis as indicated in Fig. 1(d). All experiments were carried out in a quantum design PPMS system, at magnetic fields $B \geq 2$ T and for temperatures from 5 to 300 K.

IV. RESULTS AND DISCUSSION

A. Spin-Hall magnetoresistance

Owing to the SHE, an ac-current through the Pt Hall-bar creates an ac spin accumulation at the Pt|CCO interface that can be partially absorbed or fully reflected, depending on the interface magnetization \vec{M} of the FMI (see Fig. 2(a) and (b)). The reflected spin currents generate an extra charge current via the ISHE, thereby reducing the resistance. While the longitudinal resistance establishes the maximum modulation between these two configurations with $\alpha = 0^\circ$ or 90° , the planar Hall effect vanishes. In contrast, when $\alpha = 45^\circ$, the ISHE is maximal [35], as sketched in Fig. 2(c). The additional emf scales with the applied current and is therefore, detected by the first harmonic transverse resistance R_1 [33], defined as V_1/I , where V_1 is first harmonic signal of the lock-in amplifier generated by the applied ac current amplitude I (see Appendix B for more details).

The α dependence of the first harmonic response of R_1 at 5 K in Fig. 2(d) shows on top of the expected SMR an ordinary Hall effect (OHE) generated by a magnetic field component normal to the film due to a slight misalignment of the sample by an angle β . The OHE voltage has a $\sin(\alpha + \phi)$ angular dependence, where the phase ϕ is governed by the sample tilt direction. A prefactor of $0.7 \mu\text{V}$ at a current of 2 mA in a magnetic field 6 T corresponds to a tilt of $\beta < 2^\circ$. The ordinary Hall voltage of Pt|CCO is nearly temperature independent and scales linearly with the applied current and magnetic field, as expected. After subtracting the OHE from R_1 , the anticipated $\sin 2\alpha$ dependence associated to the SMR remains [10], as illustrated in Fig. 2(d). The SMR signal, $R_{1(2\alpha)}^{\text{ampl}}$, is defined as the amplitude of the $\sin 2\alpha$ component and plotted in Fig. 2(e), (f) and (g) as a function of temperature in magnetic fields of 6 T, 4 T and 2 T, respectively. Exchanging the current and voltage probes in the Hall bar in field of 6 T leads to identical SMR profiles, confirming that the interface magnetization is parallel to the applied field. The SMR of CCO and yttrium iron garnet (YIG) are compared in Appendix C.

Below the collinear ferrimagnetic transition temperature $T_c = 94$ K, the SMR signal increases with decreasing temperature. The inset of Fig. 2(e) recorded at a magnetic field of 6 T shows a distinct change of slope at the spin-spiral transition temperature to a non-collinear magnetic phase, $T_s = 28$ K. At $T < T_s$, the SMR signal is more than one order of magnitude larger than the signal observed at T_c . A further decrease in temperature below the spin lock-in transition temperature, $T_{\text{lock-in}} = 14$ K, doubles the SMR compared to T_s . This observation indicates that the exchange interaction between metal and magnet in the Pt|CCO system is more efficient in the non-collinear spiral phase than in the collinear ferrimagnetic phase. The maximum SMR signal is observed in the spin lock-in phase, when the period of the spin spiral becomes commensurate with the lattice. Below T_c , $R_1 = A_1 T^{-1}$ (see Fig. 3(a)) gives an excellent fit, where A_1 scales linearly with the applied magnetic field, as shown in Fig. 3(b). A_1 should be proportional to the interface spin-mixing conductance that vanishes with interface magnetization. Above T_c , all magnetization is generated by the applied magnetic field and A_1 is a measure of the interface paramagnetic susceptibility. For a magnetic interface, we anticipate a bilinear $A_1(B)$, with a large slope at low magnetic fields that reflects the expulsion of magnetic domain walls. The extrapolation of the high-field data should lead to a finite cut-off at zero magnetic fields (as in studies of the anomalous Hall effect). However, the extrapolation of $A_1(B)$ does not lead to a statistically significant $A_1(0)$. At present we therefore cannot confirm whether the observed SMR signals reflect the paramagnetic susceptibility of a non-magnetic interface or a spontaneous interface magnetization texture.

In order to shed more light on the T -dependence for $T < T_c$, we compare the SMR with the bulk magnetization, as shown in Fig. 1(c). The T_c , T_s and $T_{\text{lock-in}}$ transition temperatures established from the SMR, closely corresponds to the transition temperatures observed in the bulk magnetization. In the spin-spiral and spin lock-in phases, the

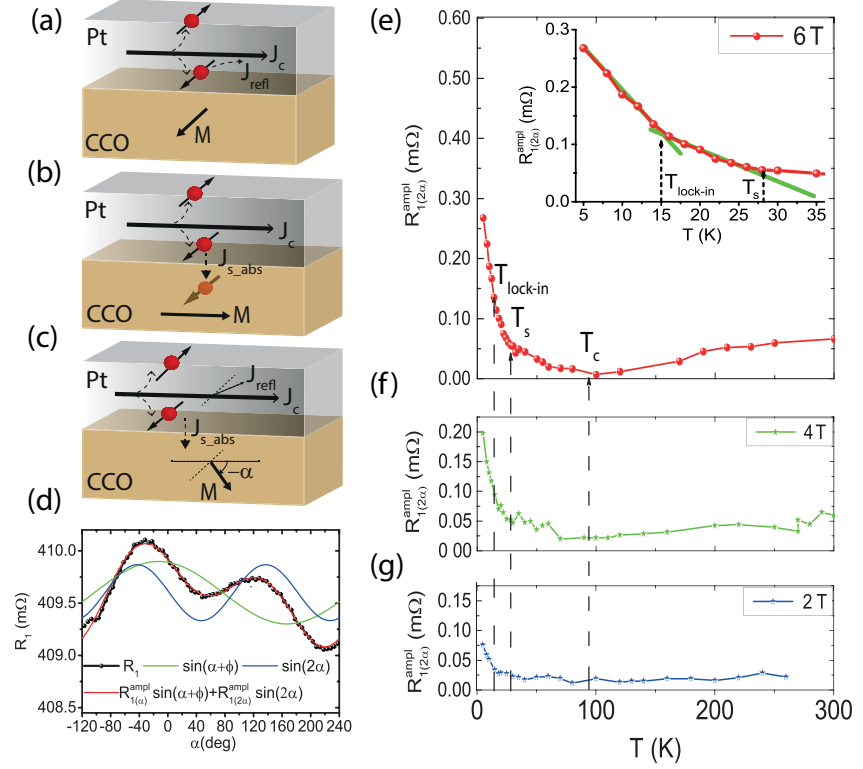


FIG. 2: (a-c) Illustration of the SMR in Pt|CCO bilayers. A charge current I induces a spin current and thereby spin accumulation at the Pt|CCO interface by virtue of the SHE. (a) This spin accumulation is absorbed as a spin transfer torque when the magnetization \vec{M} is perpendicular to the current-induced spin polarization in Pt,. (b) When \vec{M} is parallel to the spin accumulation, the spin current is reflected back into Pt, where it generates an additional charge current, J_{refl} by the ISHE. (c) When \vec{M} is at an angle α to J_c , the component of the spin accumulation perpendicular to \vec{M} is absorbed and the component parallel are reflected, leading to an extra charge current component normal to J_c that is detected in the Hall configuration (d) The angular dependence of the 1st harmonic response in the transverse configuration, $R_1 = V_1/I$, for $I = 2$ mA at 5 K in an applied magnetic field of 6 T. The $\sin(\alpha + \phi)$ and $\sin 2\alpha$ curves illustrate the additive contributions from the ordinary Hall effect and the SMR. (e), (f) and (g) show the temperature dependence of the SMR, $R_{1(2\alpha)}^{\text{ampl}}$ for $J_c = 2$ mA at 6 T, 4 T and 2 T, respectively. Here, $R_{1(2\alpha)}^{\text{ampl}}$ is the amplitude of the $\sin 2\alpha$ component from the SMR. T_c , T_s and $T_{\text{lock-in}}$ are the ferrimagnetic, spin-spiral and spin lock-in magnetic transition temperatures, respectively. The inset in (e) is a zoomed-in image of the SMR signal below T_s and $T_{\text{lock-in}}$ at 6 T.

bulk magnetization does not depend much on temperature, as shown in Fig. 1(c), in stark contrast to the SMR below T_s (Fig. 2(e)). The SMR therefore does not directly reflect the CCO bulk magnetization. Theoretically, the SMR arises from the modulation of the spin current at the NM|FMI interface by the magnetization [35] and is roughly proportional to the density of oriented magnet moments at the interface [36]. The SMR enhancement below T_s thus reflects an increased order of the magnetic moments at the interface with reduced temperature. The moments at the interface can be either Co ions, contributing to the ferrimagnetic component, or Cr ions responsible for the cycloidal component of the spin-spiral. The ferrimagnetic component of magnetization saturates around 28 K, therefore cannot explain the enhanced SMR below 28 K. However, neutron scattering experiments show that the spiral component below $T_s = 28$ K strongly depends on temperature [24], similar to the SMR signal. We therefore venture that the development of the spiral order should be explained by a strongly temperature-dependent ordering of Cr ions that cannot be observed in the global magnetization. This implies that by a simple transport experiment we can distinguish ferrimagnetic from cycloidal components of the interface magnetization.

We observe a finite SMR in the paramagnetic phase for $T > T_c$ complementing reports on spin pumping [37] and the spin Seebeck effect [8] in the paramagnetic state. In CCO the magnetic susceptibility, for $T > T_c$, follows a Curie-Weiss law with a negative Curie-Weiss temperature $\theta_{CW} = -550$ K, which is evidence for antiferromagnetic correlations. The high ratio $|\theta_{CW}|/T_c \approx 6$ indicates a significant magnetic frustration due to competing sublattice exchange interactions in CCO [32], resulting in short range order above T_c . The SMR signal above T_c increases with temperature until it saturates to a constant value around room-temperature, as shown in Fig. 2(e-g). The SMR signal

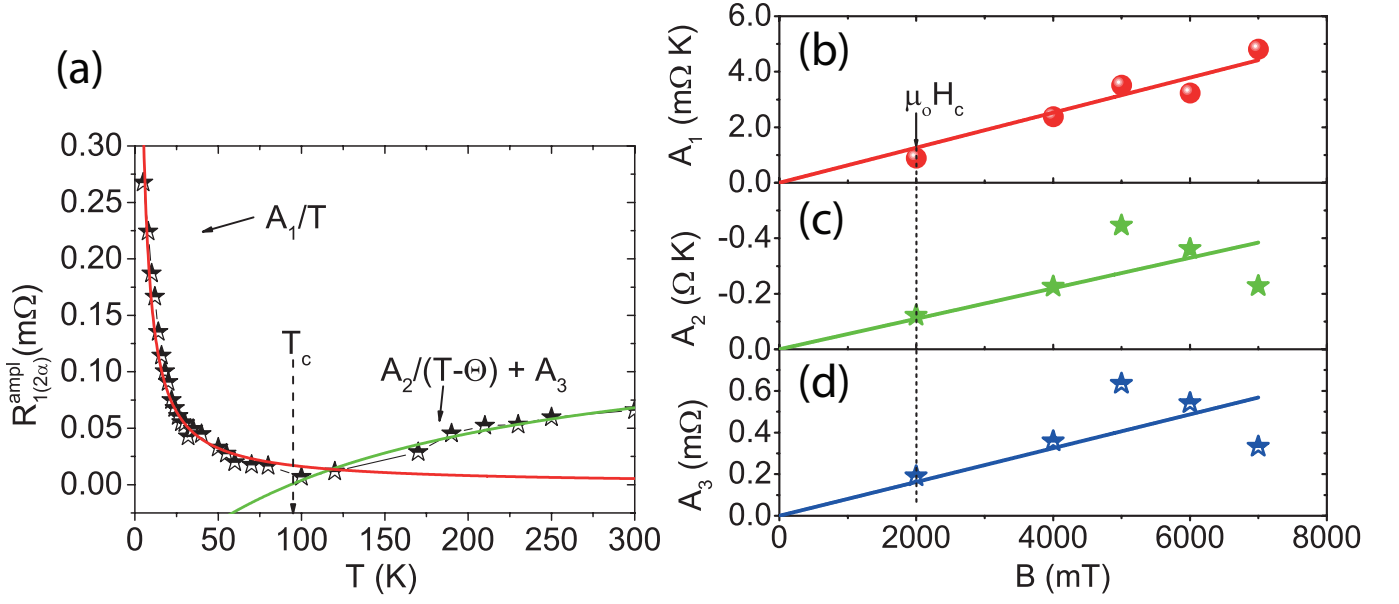


FIG. 3: (a) shows the temperature dependence of $R_{1(2\alpha)}^{ampl}$ in a magnetic field of 6 T for $I = 2$ mA. The red curve shows the fit with Curie law at low temperatures below T_c and the green curve shows the fit at the high temperature range above T_c with Curie-Weiss law (for $\theta_{CW} = -550$ K). (b), (c) and (d) show the field dependence of fitting parameters A_1 , A_2 and A_3 , respectively.

for $T > T_c$ provides evidence for an unusual interface magnetic susceptibility of our films. We fitting the SMR signals with the Curie-Weiss law, but a single fitting parameter A_2 does not capture the contributions from the molecular fields. Much unlike the bulk magnetic susceptibility, the SMR signal is suppressed at T_c which can be taking care of by introducing an additional parameter A_3 , as shown in Fig. 3(a). Both fitting parameters A_2 and A_3 scale linearly with the applied magnetic field, as shown in Fig. 3(c) and (d). This results support our conclusion drawn earlier that the SMR signal cannot be solely explained by the bulk magnetization of CCO, even in the paramagnetic phase. The temperature-independent background modelled by A_3 and the negative sign of A_2 remain unexplained by indicate that the short-range order reported for bulk CCO above T_c is importantly modified at the interface to Pt.

B. Spin Seebeck effect

We now discuss the SSE signal observed in the second harmonic response. It is caused by the Joule heating of the Pt Hall-bar, generating a heat current into the ferromagnet which is absorbed by magnons. This heat current is associated with a spin current polarized along the magnetization direction, which can be detected electrically by the ISHE, as sketched in Fig. 4(a). The second harmonic response $R_2 = \sqrt{2}V_2/I^2$, where V_2 is the second harmonic signal of the lock-in amplifier at a phase set at $\phi = -90^\circ$ [33]. The observed second harmonic response of the transverse resistance obeys the $\sin \alpha$ angular dependence anticipated for the SSE, as shown in Fig. 4(b). We define the amplitude of the $R_2^{ampl} = R_2/\sin \alpha$ for each temperature and magnetic field strength. The SSE signal for Pt/CCO has the same sign as for Pt/YIG (see Appendix C). Fig. 4(c), (d) and (e) show the temperature dependence of R_2^{ampl} in magnetic fields of 6 T, 4 T and 2 T, respectively.

In the collinear ferrimagnetic state at $T < T_c$, the SSE response increases with decreasing temperature. Fig. 4(c) gives evidence of a large SSE enhancement below the spin spiral transition temperature T_s and again below $T_{lock-in}$. The SSE signal below T_s is five times larger than the signal observed at T_c . The inset of Fig. 4(c) illustrates that the SSE at $T < T_{lock-in}$ increases by an order of magnitude from $T = 80$ K. Moreover below $T_s = 28$ K, the SSE signal scales linearly with the applied magnetic field. The SSE is too noisy to provide as clear evidence for phase transitions at T_c , T_s and $T_{lock-in}$ as the SMR signals do.

Conventional thermoelectric effects become small with decreasing temperatures, so what causes the observed remarkable enhancement at low temperatures? We can understand the temperature dependence of the SSE signal by considering the contributions from different magnetic sublattices [38, 39]. CCO is a collinear ferrimagnet above T_s , with three sublattices associated with Co and oppositely polarized Cr I and Cr II ion moments [24], but without any magnetization compensation below T_c . The magnetic sublattices contribute to the SSE by correlated thermal fluctua-

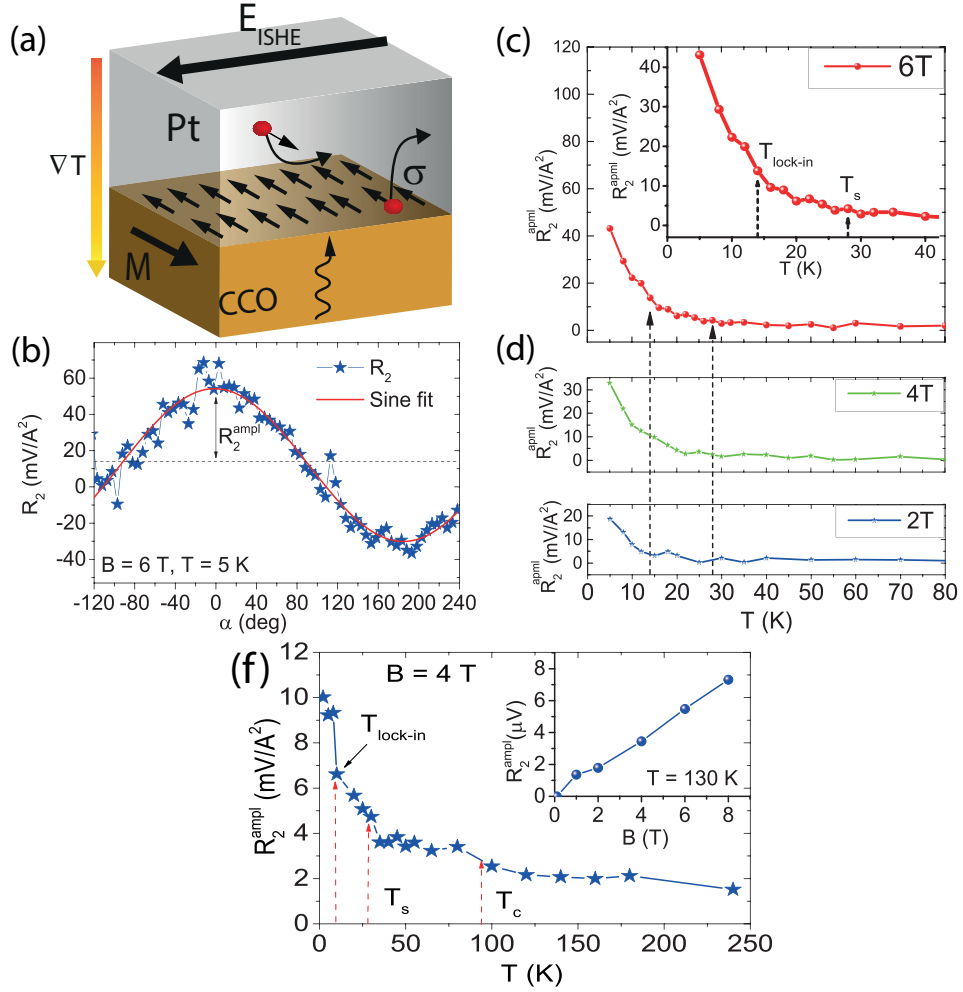


FIG. 4: (a) Spin Seebeck effect in Pt|CCO. A thermal gradient creates magnons at the interface by absorption of a spin current from Pt with polarization $\vec{\sigma} \parallel \vec{M}$, where \vec{M} is the CCO interface magnetization. The spin current generates an electromotive force \vec{E}_{ISHE} by the ISHE. (b) The angular dependence of the second harmonic response, $R_2 = \sqrt{2}V_2/I^2$ at 5 K, for $I = 2$ mA in an applied magnetic field of 6 T. (c), (d) and (e) show the temperature dependence of R_2^{ampl} at 6 T, 4 T and 2 T for $I = 2$ mA, respectively. The inset of (c) emphasizes the enhancement of the SSE signal below the spin spiral (T_s) and spin lock-in ($T_{\text{lock-in}}$) transition temperatures in a magnetic field of 6 T. (f) Temperature dependence of R_2^{ampl} in the non-linear current regime ($I = 5$ mA), with inset showing the magnetic field dependence of R_2^{ampl} at $T = 130$ K.

tions. The coupled sublattices have acoustic (ferromagnetic) and optical (antiferromagnetic) modes. The fundamental ferromagnetic modes govern the low energy excitations that are probed by ferromagnetic resonance and Brillouin light scattering. The optical modes are below T_c shifted to higher energy by the exchange interaction. In the collinear ferrimagnetic state close to T_c , the optical modes are still significantly occupied but the acoustic modes are slightly dominant. The acoustic and optical modes contribute to the SSE with different sign and therefore cancel to a large extent. By decreasing the temperature, the exchange splitting of the optical modes increases and therefore, become increasingly depleted. The suppression of the thermal pumping of the optical modes therefore, leads to an apparent enhancement of the spin Seebeck effect at lower temperature. A similar mechanism explains the low temperature sign change of the SSE of the ferrimagnetic insulator $\text{Gd}_3\text{Fe}_5\text{O}_{12}$ (GdIG) [39] and can be used to understand the temperature dependence of the SSE in YIG at temperatures above 300 K [40].

In contrast to collinear magnetic order, the magnetization texture of a spin spiral is sensitively modulated by an external magnetic field [41]. This might contribute as well to the observed magnetic field dependence of the SSE below T_s , as shown in Fig. 4(c-e). The corresponding increase in the SSE with applied magnetic field below T_s may persist until the Co^{2+} and Cr^{3+} momenta of $3\mu_B/\text{ion}$ are fully aligned. No signs of magnetization saturation were observed at magnetic fields up to 30 T [32], so it would be very interesting to find out whether also the spin Seebeck effect can be further enhanced in such high magnetic fields.

The observed correlation between the SMR and SSE provides evidence that the spin-mixing conductance, i.e., the transport measure of the exchange interaction between ferromagnet and normal metal, does play an important role. Other factors, such as the magnetization damping and the magnon transport to the interface that is affected by the magnon-phonon interaction [42], may contribute to the observed enhancement in the SSE below T_s . A quantitative description of the SSE can be approached by atomistic spin simulations that take the full spin wave spectrum associated to the three sublattices with different cone angles, chirality, and damping parameters, as well the spin mixing conductances of the interface to Pt into account.

Above T_c the SSE cannot be established at small heating current levels ($I = 2$ mA), as shown in Fig. 4(c). However, at a larger current ($I = 5$ mA) in a magnetic field of 4 T, a finite SSE signal is detected above T_c and up to room temperature, see Fig. 4(f). At these current levels, $T_{\text{lock-in}}$ is shifted to lower temperature by 4 K due to sample heating, and non-linearities kick in, i.e., the SSE voltage $\propto I^2$. The SSE still scales linearly with the applied magnetic field as shown for $T = 130$ K in the inset of Fig. 4(f). The presence of the SSE above T_c can be explained by the large longitudinal magnetic susceptibility of CCO films that is responsible for the SMR response as well [37].

In summary, by lock-in detection we simultaneously measured the SMR and SSE in Pt|CCO bilayers. The temperature dependence of the SMR and, though less so, the SSE, exposes distinct anomalies at the magnetic phase transitions. A remarkable enhancement of both SMR and SSE signals is observed at low temperatures ($T < T_s$). The SMR is more than one order of magnitude larger at $T < T_{\text{lock-in}}$ as compared to the signals around T_c . We relate the observed enhancement of the SMR below T_s to contributions from the cycloidal spiral projected onto the spin accumulation at the Pt|CCO interface. The SSE signal also increases by a factor of two when lowering temperature below T_s . The temperature dependence of the SSE does not simply reflect the bulk magnetization; instead the intricate magnetization dynamics of coupled sublattices needs to be considered. Our results suggest that the magnons from the complicated Cr-sublattice magnetization texture plays an essential role in the SSE. Vice versa, we establish that the SMR and SSE are powerful instruments that complement ferromagnetic resonance and neutron scattering techniques to analyze the magnetization dynamics of complex oxides including multiferroics.

Acknowledgments

We would like to acknowledge J. Baas, H. Bonder, M. de Roos, and J. G. Holstein for technical assistance. This work is supported by the Foundation for Fundamental Research on Matter (FOM), NanoNextNL, a micro- and nanotechnology consortium of the government of the Netherlands and 130 partners, by NanoLab NL, InSpin EU-FP7-ICT Grant No 612759 and the Zernike Institute for Advanced Materials National Research Combination, Grants-in-Aid for Scientific Research (Grant Nos. 25247056, 25220910, 26103006, and DFG Priority Programme 1538 (BA 2954/2)).

-
- [1] C. W. Sandweg, Y. Kajiwara, A. V. Chumak, A. A. Serga, V. I. Vasyuchka, M. B. Jungfleisch, E. Saitoh, and B. Hillebrands. Spin pumping by parametrically excited exchange magnons. *Phys. Rev. Lett.*, 106:216601, May 2011.
 - [2] V. Castel, N. Vlietstra, B. J. van Wees, and J. Ben Youssef. Frequency and power dependence of spin-current emission by spin pumping in a thin-film YIG/Pt system. *Phys. Rev. B*, 86:134419, Oct 2012.
 - [3] C. Hahn, G. de Loubens, M. Viret, O. Klein, V. V. Naletov, and J. Ben Youssef. Detection of microwave spin pumping using the inverse spin hall effect. *Phys. Rev. Lett.*, 111:217204, Nov 2013.
 - [4] K. Harii, T. An, Y. Kajiwara, K. Ando, H. Nakayama, T. Yoshino, and E. Saitoh. Frequency dependence of spin pumping in Pt/Y₃Fe₅O₁₂ film. *J. Appl. Phys.*, 109(11):–, 2011.
 - [5] K. Uchida, J. Xiao, H. Adachi, J. Ohe, S. Takahashi, J. Ieda, T. Ota, Y. Kajiwara, H. Umezawa, H. Kawai, G. E. W. Bauer, S. Maekawa, and E. Saitoh. Spin seebeck insulator. *Nature Mater.*, 9(11):894–897, November 2010.
 - [6] M. Schreier, A. Kamra, M. Weiler, J. Xiao, G. E. W. Bauer, R. Gross, and S. T. B. Goennenwein. Magnon, phonon, and electron temperature profiles and the spin seebeck effect in magnetic insulator/normal metal hybrid structures. *Phys. Rev. B*, 88:094410, Sep 2013.
 - [7] A. Aqeel, I. J. Vera-Marun, B. J. van Wees, and T. T. M. Palstra. Surface sensitivity of the spin seebeck effect. *J. Appl. Phys.*, 116(15):153705, 2014.
 - [8] S. M. Wu, J. E. Pearson, and A. Bhattacharya. Paramagnetic spin seebeck effect. *Phys. Rev. Lett.*, 114:186602, May 2015.
 - [9] J. Flipse, F. K. Dejene, D. Wagenaar, G. E. W. Bauer, J. Ben Youssef, and B. J. van Wees. Observation of the spin peltier effect for magnetic insulators. *Phys. Rev. Lett.*, 113:027601, Jul 2014.
 - [10] M. Althammer, S. Meyer, H. Nakayama, M. Schreier, S. Altmannshofer, M. Weiler, H. Huebl, S. Geprägs, M. Opel, R. Gross, D. Meier, C. Klewe, T. Kuschel, J. Schmalhorst, G. Reiss, L. Shen, A. Gupta, Y.-T. Chen, G. E. W. Bauer, E. Saitoh, and S. T. B. Goennenwein. Quantitative study of the spin hall magnetoresistance in ferromagnetic insulator/normal metal hybrids. *Phys. Rev. B*, 87:224401, Jun 2013.

- [11] N. Vlietstra, J. Shan, V. Castel, B. J. van Wees, and J. Ben Youssef. Spin-hall magnetoresistance in platinum on yttrium iron garnet: Dependence on platinum thickness and in-plane/out-of-plane magnetization. *Phys. Rev. B*, 87:184421, May 2013.
- [12] H. Nakayama, M. Althammer, Y.-T. Chen, K. Uchida, Y. Kajiwara, D. Kikuchi, T. Ohtani, S. Geprags, M. Opel, S. Takahashi, R. Gross, G. E. W. Bauer, S. T. B. Goennenwein, and E. Saitoh. Spin hall magnetoresistance induced by a nonequilibrium proximity effect. *Phys. Rev. Lett.*, 110:206601, May 2013.
- [13] N. Vlietstra, J. Shan, V. Castel, J. Ben Youssef, G. E. W. Bauer, and B. J. van Wees. Exchange magnetic field torques in YIG/Pt bilayers observed by the spin-hall magnetoresistance. *Appl. Phys. Lett.*, 103(3):–, 2013.
- [14] C. Hahn, G. de Loubens, O. Klein, M. Viret, V. V. Naletov, and J. Ben Youssef. Comparative measurements of inverse spin hall effects and magnetoresistance in YIG/Pt and YIG/Ta. *Phys. Rev. B*, 87:174417, May 2013.
- [15] M. Isasa, A. Bedoya-Pinto, S. Velez, F. Golmar, F. Sanchez, L. E. Hueso, J. Fontcuberta, and F. Casanova. Spin hall magnetoresistance at Pt/CoFe₂O₄ interfaces and texture effects. *Appl. Phys. Lett.*, 105(14):–, 2014.
- [16] J. H. Han, C. Song, F. Li, Y. Y. Wang, G. Y. Wang, Q. H. Yang, and F. Pan. Antiferromagnet-controlled spin current transport in SrMnO₃/Pt hybrids. *Phys. Rev. B*, 90:144431, Oct 2014.
- [17] M. Fiebig. Revival of the magnetoelectric effect. *J. Phys. D: Appl. Phys.*, 38(8):R123, 2005.
- [18] Sang-Wook Cheong and Maxim Mostovoy. Multiferroics: a magnetic twist for ferroelectricity. *Nature Mater.*, 6(1):13–20, 2007.
- [19] Y. Tokura and S. Seki. Multiferroics with spiral spin orders. *Adv. Mater.*, 22(14):1554–1565, 2010.
- [20] R. Ramesh and N. A. Spaldin. Multiferroics: progress and prospects in thin films. *Nature Materials*, 6(1):21–9, 2007.
- [21] T. Kimura and Y. Tokura. Magnetoelectric phase control in a magnetic system showing cycloidal/conical spin order. *J. Phys.: Condens. Matter*, 20(43):434204, 2008.
- [22] Y. Yamasaki, S. Miyasaka, Y. Kaneko, J.-P. He, T. Arima, and Y. Tokura. Magnetic reversal of the ferroelectric polarization in a multiferroic spinel oxide. *Phys. Rev. Lett.*, 96:207204, May 2006.
- [23] Y. J. Choi, J. Okamoto, D. J. Huang, K. S. Chao, H. J. Lin, C. T. Chen, M. van Veenendaal, T. A. Kaplan, and S-W. Cheong. Thermally or magnetically induced polarization reversal in the multiferroic cocr₂O₄. *Phys. Rev. Lett.*, 102:067601, Feb 2009.
- [24] K. Tomiyasu, J. Fukunaga, and H. Suzuki. Magnetic short-range order and reentrant-spin-glass-like behavior in CoCr₂O₄ and MnCr₂O₄ by means of neutron scattering and magnetization measurements. *Phys. Rev. B*, 70:214434, Dec 2004.
- [25] S. Bordacs, D. Varjas, I. Kezsmarki, G. Mihaly, L. Baldassarre, A. Abouelsayed, C. A. Kuntscher, K. Ohgushi, and Y. Tokura. Magnetic-order-induced crystal symmetry lowering in acr₂O₄ ferrimagnetic spinels. *Phys. Rev. Lett.*, 103:077205, Aug 2009.
- [26] S. Yang, H. X. Bao, D. Z. Xue, C. Zhou, J. H. Gao, Y. Wang, J. Q. Wang, X. P. Song, Z. B. Sun, X. B. Ren, and K. Otsuka. Magnetodielectric effect from the onset of ferrimagnetic transition in CoCr₂O₄. *J. Phys. D: Appl. Phys.*, 45(26):265001, 2012.
- [27] G. Lawes, B. Melot, K. Page, C. Ederer, M. A. Hayward, Th. Proffen, and R. Seshadri. Dielectric anomalies and spiral magnetic order in CoCr₂O₄. *Phys. Rev. B*, 74:024413, Jul 2006.
- [28] K. Singh, A. Maignan, C. Simon, and C. Martin. FeCr₂O₄ and CoCr₂O₄ spinels: Multiferroicity in the collinear magnetic state? *Appl. Phys. Lett.*, 99(17):–, 2011.
- [29] Mufti N., A. A. Nugroho, G. R. Blake, and T. T. M. Palstra. Magnetodielectric coupling in frustrated spin systems: the spinels MCr₂O₄ (M = Mn, Co and Ni). *Journal of Physics: Condensed Matter*, 22(7), 2010-2-24.
- [30] K. R. Choi, S. J. Moon, T. Kouh, I. B. Shim, S. J. Kim, and C. S. Kim. Characterization of CoCr₂O₄ on Pt(111) grown by using pulsed laser deposition. *IEEE Trans. Magn.*, 45(6):2610–2612, June 2009.
- [31] Xiaoran Liu, M. Kareev, Yanwei Cao, Jian Liu, S. Middey, D. Meyers, J. W. Freeland, and J. Chakhalian. Electronic and magnetic properties of (1 1 1)-oriented CoCr₂O₄ epitaxial thin film. *Appl. Phys. Lett.*, 105(4):–, 2014.
- [32] V. Tsurkan, S. Zherlitsyn, S. Yasin, V. Felea, Y. Skourski, J. Deisenhofer, H.-A. Krug von Nidda, J. Wosnitza, and A. Loidl. Unconventional magnetostructural transition in CoCr₂O₄ at high magnetic fields. *Phys. Rev. Lett.*, 110:115502, Mar 2013.
- [33] N. Vlietstra, J. Shan, B. J. van Wees, M. Isasa, F. Casanova, and J. Ben Youssef. Simultaneous detection of the spin-hall magnetoresistance and the spin-seebeck effect in platinum and tantalum on yttrium iron garnet. *Phys. Rev. B*, 90:174436, Nov 2014.
- [34] M. Schreier, N. Roschewsky, E. Dobler, S. Meyer, H. Huebl, R. Gross, and S. T. B. Goennenwein. Current heating induced spin seebeck effect. *Appl. Phys. Lett.*, 103(24):–, 2013.
- [35] Y.-T. Chen, S. Takahashi, H. Nakayama, M. Althammer, S. T. B. Goennenwein, E. Saitoh, and G. E. W. Bauer. Theory of spin hall magnetoresistance. *Phys. Rev. B*, 87:144411, Apr 2013.
- [36] Xingtao Jia, Kai Liu, Ke Xia, and Gerrit E. W. Bauer. Spin transfer torque on magnetic insulators. *Europhys. Lett.*, 96(1):17005, October 2011.
- [37] Y. Shiomi and E. Saitoh. Paramagnetic spin pumping. *Phys. Rev. Lett.*, 113:266602, Dec 2014.
- [38] Y. Ohnuma, H. Adachi, E. Saitoh, and S. Maekawa. Spin seebeck effect in antiferromagnets and compensated ferrimagnets. *Phys. Rev. B*, 87:014423, Jan 2013.
- [39] S. Geprags, A. Kehlberger, T. Schulz, C. Mix, F. D. Coletta, S. Meyer, A. Kamra, M. Althammer, G. Jakob, H. Huebl, R. Gross, S. T.B. Goennenwein, and M. Klui. Origin of the spin seebeck effect probed by temperature dependent measurements in Gd₃Fe₅O₁₂. *ArXiv e-prints*, 2014.
- [40] K. Uchida, T. Kikkawa, A. Miura, J. Shiomi, and E. Saitoh. Quantitative temperature dependence of longitudinal spin seebeck effect at high temperatures. *Phys. Rev. X*, 4:041023, Nov 2014.
- [41] D. Kamenskiy, H. Engelkamp, T. Fischer, M. Uhlarz, J. Wosnitza, B. P. Gorshunov, G. A. Komandin, A. S. Prokhorov,

- M. Dressel, A. A. Bush, V. I. Torgashev, and A. V. Pronin. Observation of an intersublattice exchange magnon in CoCr_2O_4 and analysis of magnetic ordering. *Phys. Rev. B*, 87:134423, Apr 2013.
- [42] V. I. Torgashev, A. S. Prokhorov, G. A. Komandin, E. S. Zhukova, V. B. Anzin, V. M. Talanov, L. M. Rabkin, A. A. Bush, M. Dressel, and B. P. Gorshunov. Magnetic and dielectric response of cobalt-chromium spinel CoCr_2O_4 in the terahertz frequency range. *Phys. Solid State*, 54(2):350–359, 2012.
- [43] S. R. Marmion, M. Ali, M. McLaren, D. A. Williams, and B. J. Hickey. Temperature dependence of spin hall magnetoresistance in thin YIG/Pt films. *Phys. Rev. B*, 89:220404, Jun 2014.
- [44] S. Meyer, M. Althammer, S. Geprags, M. Opel, R. Gross, and S. T. B. Goennenwein. Temperature dependent spin transport properties of platinum inferred from spin hall magnetoresistance measurements. *Appl. Phys. Lett.*, 104(24):–, 2014.

Appendix A: CCO film magnetization

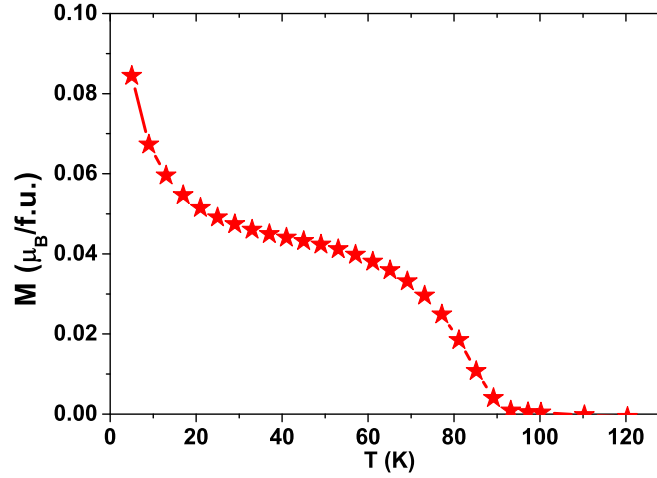


FIG. 5: In-plane magnetization of a CCO film on a MgO substrate in a magnetic field of 0.01 T after cooling in 1 T.

The temperature-dependent magnetization of the CCO film in Fig. 5 as measured by SQUID magnetometry is evidence for a phase transition at $T_c = 94\text{K}$ to collinear ferrimagnet order, but the spin-spiral and spin lock-in transitions are not visible, because of the small magnetization of a thin film as explained in the main text. The apparent increase in the magnetization below 20 K is probably caused by paramagnetic impurities in the substrate.

Appendix B: Lock-in detection

All measurements shown in the main text are carried out using a lock-in detection technique [33] with $I \leq 5\text{mA}$ ac current bias in the Pt film. The generated voltage can be expanded as

$$V(t) = R_1 I(t) + R_2 I^2(t) + R_3 I^3(t) + \dots, \quad (\text{B1})$$

where R_n represent the n -th harmonic response. For $I(t) = \sqrt{2}I_0 \sin \omega t$, with angular frequency ω and rms value I_0 , the harmonic response coefficients R_n are obtained by measuring the different frequency components ($1\omega, 2\omega, \dots$) by a lock-in amplifier. The detected n -th harmonic response at a set phase ϕ can be written as

$$V_n(t) = \frac{\sqrt{2}}{T} \int_{t-T}^t \sin(n\omega s + \phi) V(s) ds. \quad (\text{B2})$$

Focussing on first and second order response, we define the output voltage of the lock-in amplifier for the first and second harmonic responses by using Eq. (B1) and Eq. (B2) as:

$$\begin{aligned} V_1 &= I_0 R_1 & \text{for } \phi &= 0^\circ \\ V_2 &= I_0^2 R_2 / \sqrt{2} & \text{for } \phi &= -90^\circ \end{aligned} \quad (\text{B3})$$

The SMR and the SSE signals appear in the first and second harmonic responses in Eq. (B3), respectively.

In the linear response regime at currents $I \leq 2$ mA, the SMR scales linearly and the SSE scales quadratically with the applied current as shown in Fig. 6(a,b). However, at $I > 2$ mA, the SMR (SSE) do no longer depend linearly (quadratically) on the current I . The results in the main text for the SMR are gathered in the linear regime. At $T > T_s$ the SSE signal decreases rapidly and we record the SSE also at the high current $I = 5$ mA, as shown in Fig. 6(c).

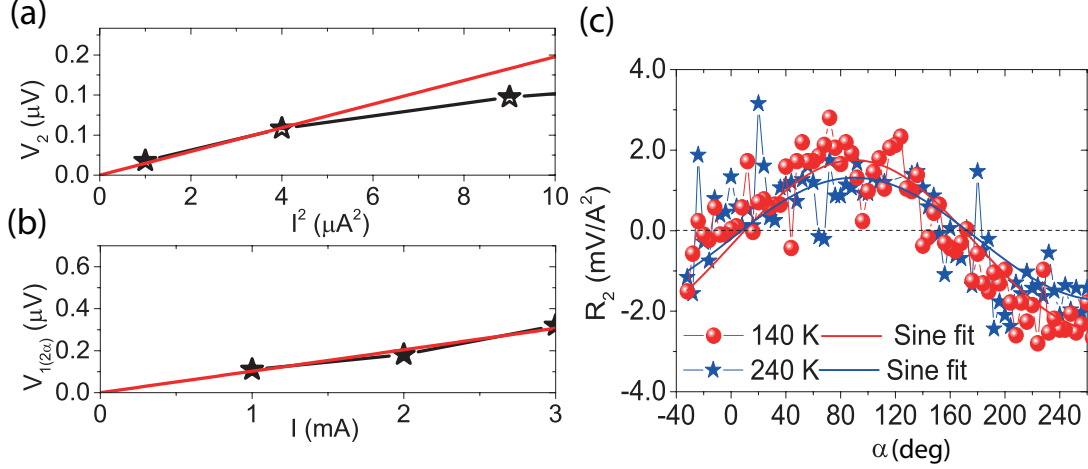


FIG. 6: (a) Dependence of the second harmonic response V_2 on I^2 due to the SSE, generated by current induced heating and (b) dependence of first harmonic contribution $V_{1(2\alpha)}$, due to the SMR, by an ac-current I sent through the Pt Hall-bar in a magnetic field of 4 T. The SMR scales linear and the SSE scales quadratic I in the linear-regime ($I \leq 2$ mA). (c) The angular dependence of second harmonic response, R_2 , for $I = 5$ mA, $H = 4$ T at $T = 140$ K and 240 K.

Appendix C: SMR and the SSE in Pt|YIG vs. Pt|CCO

To compare the SMR and the SSE response in Pt|CCO system to that of Pt|YIG, the angular dependence of Pt|YIG system is also systematically studied at different temperatures. A 4 nm-thick Pt Hall-bar was deposited on a 4×4 mm² YIG film by dc sputtering [33]. The Pt Hall-bar has a length of 500 μm and a width of 50 μm , with side contacts of 10 μm width. A 200 nm thick YIG, single-crystal, film is used and the film is grown by liquid phase epitaxy on a (111) $\text{Gd}_3\text{Ga}_5\text{O}_{12}$ (GGG) substrate.

We observe the same sign of the SMR signals for Pt|CCO and Pt|YIG, as expected. A change of the sign of SSE has been observed in compensated ferrimagnet [39] but for both Pt|YIG and Pt|CCO system the sign remains the normal for all temperatures (5 – 300 K).

The temperature dependence of the SMR and SSE is observed to be very different in the Pt|CCO as compared to the Pt|YIG system. In Pt|CCO, both SMR and the SSE signals are enhanced at temperatures much lower than T_c , as shown in Fig. 2(e) and Fig. 4(c) with maximal values around 5 K in the spin lock-in phase. In contrast, Pt|YIG displays conventional behavior, with both SMR and SSE larger at room temperature than at low temperatures. Fig. 7(a) shows the temperature dependence Pt|YIG SMR at relatively large current levels of $I = 2.5$ mA. The SMR signal slightly increases when decreasing temperature until 150 K and decreases again when cooling even more [43]. The decrease in the SMR signal in Pt|YIG has been ascribed to a decrease in the Pt spin-Hall angle with decreasing temperature [44]. The SMR signal observed at 5 K is twice smaller than that at room-temperature. The SSE in Pt|YIG does not change much until $T = 200$ K, while a further decrease in temperature suppresses the SSE as shown in Fig. 7(b). A small increase in the SSE is observed for $T < 30$ K.

The ordinary Hall effect as observed in the first harmonic response of transverse resistance (as shown in Fig. 2(d)) is almost temperature independent in Pt|CCO system and scales linearly with the applied field as expected. The ordinary Hall effect is not observed in the Pt|YIG system because a much weaker field suffice to saturate the YIG magnetization ($H_c < 1$ mT). Moreover, the SMR signal observed in the Pt|CCO (shown in Fig. 2(e)) is smaller than that in the Pt|YIG system, resulting in a relatively larger contribution of the ordinary Hall effect. The SMR response observed at 5 K in the Pt|CCO is more than one order of magnitude smaller than the signal observed in the Pt|YIG.

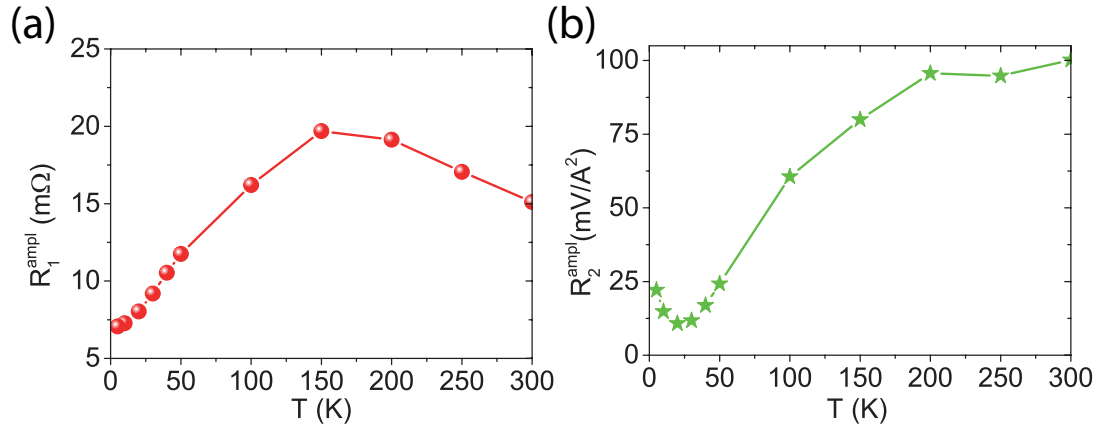


FIG. 7: (a) Temperature dependence of the SMR and (b) the SSE in the Pt|YIG system for 2.5 mA current through the Pt Hall-bar in a magnetic field of 0.1 T.